Automated Extraction of Street Lights From JL1-3B Nighttime Light Data and Assessment of Their Solar Energy Potential

Bin Cheng, Zuoqi Chen, *Member, IEEE*, Bailang Yu, *Senior Member, IEEE*, Qiaoxuan Li, Congxiao Wang, Beibei Li, Bin Wu, Yong Li, and Jianping Wu

***Abstract*—To realize energy conservation and environmental protection, solar street lights have been widely used in urban areas in China. To reasonably and effectively utilize solar street lights, the original street lights must be located, and the solar street light potential must be assessed. The Jilin1-03B (JL1-3B) satellite provides next-generation nighttime light data with a high spatial resolution and in three spectral bands. Consequently, the street lights can be extracted from the nighttime light data. We used the road network dataset from the open street map with a specific buffer to extract the road area as a constraint region. Next, the grayscale brightness of JL1-3B images was obtained by integrating all the three bands to locate the street light by using a local maximum algorithm. Then, the values of the original three bands were utilized to classify the types of street lights as high-pressure sodium (HPS) lamps or light-emitting diode lamps. Finally, we simulated the replacement of all the HPS lamps with solar street lights and assessed the corresponding solar energy potential by using the digital surface model data and hourly cloud cover data through the SHORTWAVE-C model. The accuracy of location of the street lights was approximately 90%. Replacing an HPS lamp by one solar street light for 20 years can save 1.85×10^4 kWh of electrical energy, 7.41 t of standard coal, 5.03 t of C emissions, 18.47 t of CO_2 emissions, 0.55 t of SO_2 emissions, and 0.28 t of NO_X emissions.**

***Index Terms*—Jilin1-03B (JL1-3B) satellite, nighttime light, solar energy potential, street light.**

I. Introduction

With the development of society, the demand for energy is increasing. At present, China's energy consumption structure involves mainly fossil energy [1], which may lead to energy shortages and environmental pollution [2]. Owing to the limited energy reserves and occurrence of severe environment problems, energy conservation has become a major concern [3]. Because of the continuous urban expansion, the energy consumption for urban lighting has increased rapidly [4], [5]. According to the National Energy Administration statistics, the annual electricity consumption for urban lighting accounts for 4% to 5% of the total electricity consumption in China [6]. Street lights are a dominant component of urban lighting, and they should be considered and promptly assessed for urban energy conservation in the context of urban planning, especially in large-scale cities.

In most of the cities in China, high-pressure sodium (HPS) lamps are the primary choice for street lighting [7]. HPS lamps are powered by fossil energy, which could lead to serious environment issues. Many cities have started using energy-efficient street lights to replace the traditional HPS lamps for street lighting [8]. Solar street lights are powered by crystalline silicon solar cells, and the electrical energy of these cells is stored in a valve-controlled battery. Solar street lights, which use light-emitting diode (LED) lamps as the light source, exploit the advantages of both solar energy and LED lamps [9]. Because of its energy saving ability, solar street lights have become the future of urban lighting [10]. With sufficient solar energy, some researchers have successfully demonstrated the replacement of traditional HPS street lights by solar street lights to provide road lighting because traditional HPS street lights consume fossil fuel and pollute the environment [11].

To assess the potential of solar street lights, first, the specific location of the street lights must be determined and the lights that need to be replaced must be identified by determining their lamp types. Traditionally, field surveys were used to record the specific location and type of street lights; however, this process requires a large amount of labor and time. To overcome these drawbacks, researchers attempted to extract street lights from

Manuscript received September 22, 2019; revised December 3, 2019 and January 21, 2020; accepted January 27, 2020. Date of publication February 4, 2020; date of current version February 20, 2020. This work was supported in part by the National Natural Science Foundation of China under Grant 41871331 and Grant 41801343, in part by the Fundamental Research Funds for the Central Universities of China, in part by the ECNU Academic Innovation Promotion Program for Excellent Doctoral Students under Grant YBNLTS2019-001, and in part by the Chang Guang Satellite Technology Company, Ltd. *(Bin Cheng and Zuoqi Chen are co-first authors.) (Corresponding author: Bailang Yu.)*

Bin Cheng, Bailang Yu, Qiaoxuan Li, Congxiao Wang, Bin Wu, Yong Li, and Jianping Wu are with the Key Laboratory of Geographic Information Science Ministry of Education and the School of Geographic Sciences, East China Normal University, Shanghai 200241, China (e-mail: cb476173047@163.com; blyu@geo.ecnu.edu.cn; leejoetion@gmail.com; cxwang1992@126.com; bwu@geo.ecnu.edu.cn; ly_ecnu@outlook.com; jpwu@geo.ecnu.edu.cn).

Zuoqi Chen is with the Key Laboratory of Spatial Data Mining and Information Sharing of Ministry of Education, National & Local Joint Engineering Research Center of Satellite Geospatial Information Technology and the Academy of Digital China, Fuzhou University, Fuzhou 35002, China (e-mail: zqchen@fzu.edu.cn).

Beibei Li is with Chang Guang Satellite Technology Company, Ltd., and Changchun Institute of Optics, Fine Mechanics and Physics, Chinese Academy of Sciences, Jilin 130033, China (e-mail: libeibei0208@163.com).

Digital Object Identifier 10.1109/JSTARS.2020.2971266

other data. Because the size of a street light is small, street light extraction is usually performed using data with a high spatial resolution data, for instance, vehicle-borne light detection and ranging (LiDAR) data [12]. Existing research can be divided into the following four categories.

1) Spatial clustering of vehicle-borne LiDAR data: on the premise of filtering ground information, LiDAR spatial clusters were extracted and classified into different categories (e.g., street light, building, and tree) according to the spatial characteristics of the clusters [13], [14].
2) Geometric characteristics of ground objects: the semantic information and some arbitrary criteria were utilized for extracting and classifying rod-shaped objects [15], [16]. However, the accuracy of these two methods can be limited by the performance of distinguishing the street lights and other rod-shaped objects (e.g., trees, signs, and telegraph-poles).
3) Supervoxel segmentation of point cloud dataset: this method involves collecting the spatial information within a moving window and then determining the specific spatial information of a street light as reference. The street light can then be extracted by comparing the information similarity between each moving window and reference street light region. This method can effectively overcome the disadvantages of occlusion and data incompleteness and distinguish light poles, traffic signs, vehicles, and other objects [17], [18].
4) Graph matching: the method first employs automatic training or establishes an *a priori* sample. Subsequently, with the support of geometric constraints and semantic information, the categories of target objects can be determined from a three-dimensional scene. This method can accurately extract various types of ground objects, including street lights [19], [20].

Although vehicle-borne LiDAR has been successfully used to extract the shape and position of street lights, the slender shape of street light renders the LiDAR data in the street light region as having a low point cloud density and poor data integrity, which can generally reduce the extraction accuracy. Furthermore, vehicle-borne LiDAR data is too expensive to be suitable for large-scale scenes [18], and it cannot identify the street light type. Therefore, it is necessary to develop a novel alternative that can be applied to extract a street light within a large region.

Nighttime light data, as an emerging remote sensing data source, can act as a new data source for urban research [21]–[24]. The Defense Meteorological Satellite Program-Operational Linescan System (DMSP-OLS), Suomi National Polar-Orbiting Partnership Visible Infrared Imaging Radiometer Suite (NPP-VIIRS), and Luojia 1-01 satellite (LJ1-01), as three main sources of nighttime light remote sensing data, are widely used in large-scale urban research [25]–[28]. However, because of their coarse spatial resolution and the lack of multispectral information, DMSP-OLS, NPP-VIIRS, and LJ1-01 nighttime light data do not have the capacity to locate a street light and distinguish its light type. Jilin1-03B (JL1-3B), as a novel generation of commercial nighttime satellites, has a better spatial resolution ($\sim$0.92 m) and can provide multispectral information. It offers the possibility to study the street light infrastructure at a finer scale.[1] Zheng *et al*. [29] evaluate the ability of JL1-3B nighttime light data for monitoring the spatial pattern and discriminating the types of artificial light based on a case study of Hangzhou, China; however, they did not locate the light position.

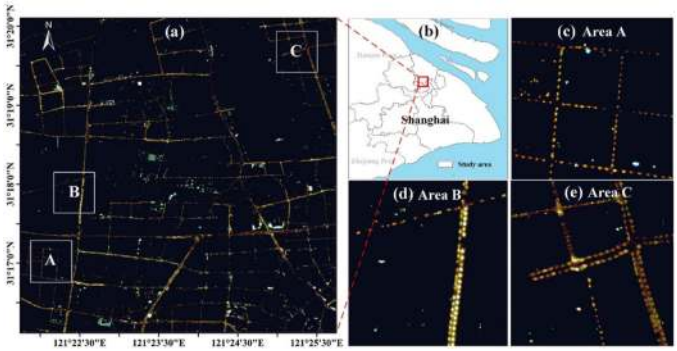

Fig. 1. (a) JL1-3B nighttime light image in the study area. (b) Location of study area. (c)–(e) Three sample areas A, B, and C, respectively.

To this end, in this article, we present an approach to automatically extract street lights from JL1-3B nighttime light data and assess the corresponding solar energy potential from a digital surface model (DSM). The remaining of this article is organized as follows. A detailed description of the study area and datasets is provided in Section II. Section III introduces the methods applied to locate street lights, recognize their lamp type, and assess the solar street light utilization potential. The results and discussion are presented in Sections IV and V, respectively, and the conclusions are presented in Section VI.

II. Study Area and Datasets

A. Study Area

Shanghai [see Fig. 1(b)], which is situated on the Yangtze River Economic Belt, is one of the most prosperous cities in China. It has a humid subtropical climate with sufficient sunshine. Considering the JL1-3B nighttime light data quality (cloud cover ratio and noise proportion) and the street light distribution, a rectangular area located in northern Shanghai was selected for our case study [see Fig. 1(a)] as this region encompasses several street lights with different light types. The study area has a size of 51.03 km^2 and a relatively flat terrain. In addition, three sample areas, namely, areas A [(see Fig. 1(c)], B [see Fig. 1(d)], and C [see Fig. 1(e)] were selected to evaluate the results of street light extraction and classification. It is worth noting that this study area is much larger than the conventionally used study areas, like road segments, when vehicle-borne LiDAR are used to perform similar tasks.

B. Datasets

Chang Guang Satellite Technology, Company, Ltd. launched the JL1-3B satellite on January 9, 2017. JL1-3B is on a sun-synchronous orbit with an altitude of 535 km. Compared with

[1][Online]. Available: http://mall.charmingglobe.com/dataShow.html

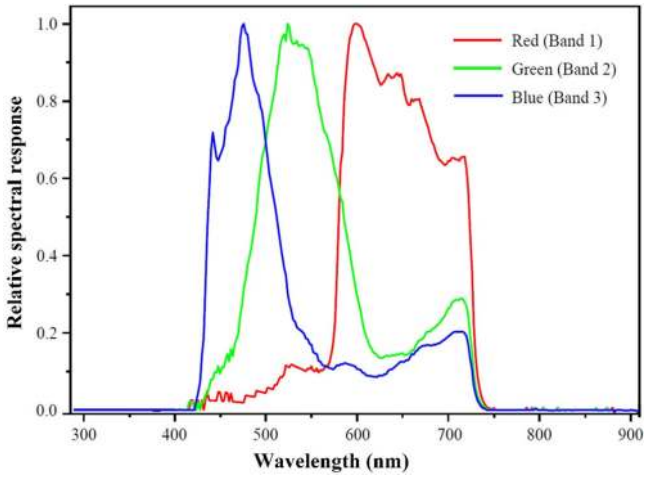

Fig. 2. Relative spectral response of JL1-3B.

TABLE I
TEST RESULTS OF SPECTRAL CHARACTERISTIC PARAMETERS (UNIT: NM)

Band	Peak wavelength	Half peak beginning	Half peak ending	Half peak width
R	598	580	723	143
G	524	489	585	96
B	476	437	512	75

the DMSP-OLS and NPP-VIIRS, JL1-3B has two outstanding advantages: first, higher spatial resolution of ∼0.92 m and, second, multispectral bands including a blue band (437–512 nm), green band (489–585 nm), and red band (580–723 nm) [29]. The relationship between the relative spectral response and wavelength of JL1-3B is shown in Fig. 2. Table I lists the peak wavelength, half peak beginning, half peak ending, and half peak width of the three bands in the JL1-3B nighttime light data. These data have been acquired through an official preprocess to enhance its quality, including radiance correction, geometric correction, and orthorectification. The JL1-3B nighttime light data captured on September 1, 2017, with an overpass time of around 22:12 local time and a satellite zenith angle of around 30°, were used to locate the street lights and classify their lamp types. From Fig. 1, some unusual bright spots were found near the road, which was always caused by the decorative light outside the buildings and was found to affect our accuracy. Therefore, a preprocess was designed to handle it and will be introduced in Section III.

The sky quality meter (SQM), which is a low-cost and pocket-sized night-sky brightness photometer, was used to detect the changes in the luminance on the road, and included a GPS to record the specific location. The SQM measures the amount of incoming light as brightness values in logarithmic units of magnitude per square second of arc (mag/arcsec^2) and higher values represent a lower brightness [30]. The SQM was positioned on a specially designed pole at a height of 1.5 m in the downward direction in uniform motion.

The open street map (OSM) road network data[2] were used to generate a road area mask as a constraint region and ensure

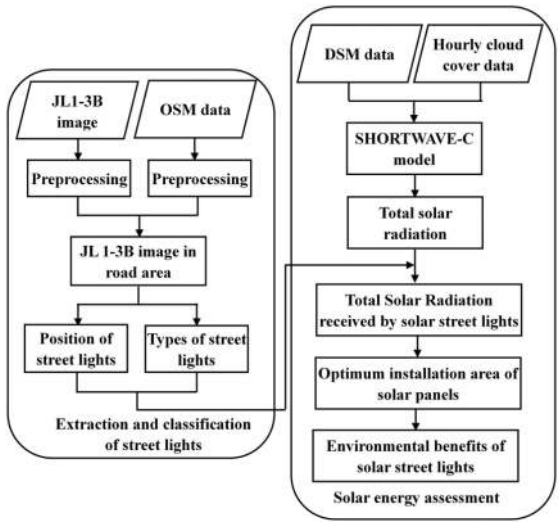

Fig. 3. Workflow of the proposed approach.

that the extracted street lights are located in the road area. However, because the OSM data is a free editable map of the world, it could have some errors [31]. Consequently, by visually interpreting Google Earth images, the OSM road network data were corrected manually in aspects of geometry and spatial reference.

The DSM data in 2016 and hourly cloud cover data in 2016 were applied to calculate the spatiotemporal distribution of the solar radiation data for further assessment of solar street light utilization. The DSM data were provided by the Shanghai Municipal Institute of Surveying and Mapping, and the spatial resolution of the DSM data was 0.5 m. Hourly cloud cover data from January 1 to December 31, 2016 were downloaded from the National Meteorological Information Center.[3]

III. METHOD

A two-part approach is proposed for extracting street lights and assessing the solar street light utilization potential (see Fig. 3). Part 1 involves generating the road area mask from the OSM data, integrating the three bands of the JL1-3B image for pinpointing street lights, and distinguishing the light type (HPS or LED lamps). Part 2 involved assessing the solar street light utilization potential. In this part, the SHORTWAVE-C model [32] was applied to estimate the solar radiance for each street light and assess the solar street light utilization potential considering the corresponding received solar radiance and the optimum installation area of the solar panels.

A. Extraction and Classification of Street Lights

To formulate a method to locate the positions of street lights, the SQM device was orientated downward in the field to record the luminance along the road edge (close to street lights) and this was used to analyze the spatial variance impacted by the street light. Fig. 4(a) shows a sample of the field survey, and Fig. 4(b)

[2][Online]. Available: https://www.openstreetmap.org

[3][Online]. Available: http://data.cma.cn/

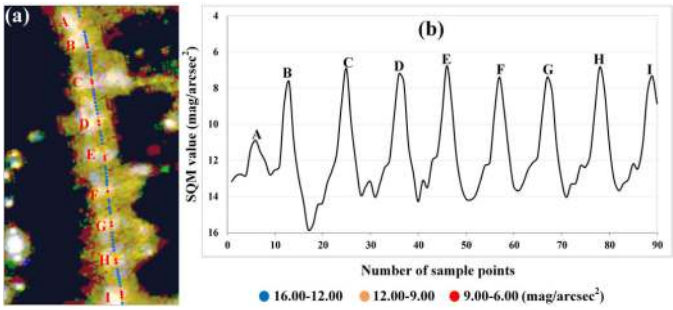

Fig. 4. (a) JL1-3B nighttime light image of sample points and (b) SQM values of sample points.

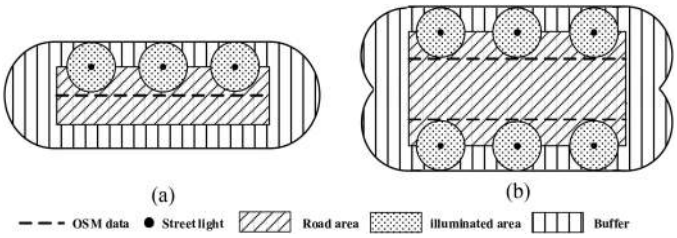

Fig. 5. Buffer range, illuminated area, and two different road areas.

displays the SQM values of the sample points. In total, nine peaks were found, as shown in Fig. 4(b), which correspond to the nine street lights (A–I) shown in Fig. 4(a). This situation implies that the extraction of street lights can be considered as determining each local peak position, namely the local maximum nighttime light intensity brightness.

After radiometric calibration was applied on JL1-3B with metadata files, the original digital number (DN) value was converted to the radiance of each band. To reduce the georeferencing error, the JL1-3B data and DSM data were projected to the Universal Transverse Mercator projection system with a spatial resolution of 1 m. To quantify the total radiation of the three bands, the grayscale brightness of JL1-3B was calculated using [33]

$$\text{Brightness} = 0.2989 \times \text{Band}_R + 0.5870 \times \text{Band}_G + 0.1140 \times \text{Band}_B \quad (1)$$

where Brightness represents the grayscale brightness of JL1-3B. Band_R, Band_G, and Band_B represent the radiances of the red, green, and blue bands, respectively.

To eliminate the light intensity from the nonroad areas to ensure that the extracted street lights are located in the road area, the road network from the OSM with a specific buffer was mapped as the road area mask. According to the characteristics of OSM data, one line (dashed line in Fig. 5) represents a road within a width of approximately 20 m and a road width of more than 20 m is indicated as two or more lines. Therefore, the buffer generated by the roads in the first case must cover the entire road and a little region outside the road to ensure that the light source exists in the buffer area [see Fig. 5(a)]. In the second case, the buffer generated by one line needs to cover the road and the areas illuminated by the street lights on one side [see Fig. 5(b)]. Considering the width of the roads and radius of the areas illuminated by the street lights in the considered study area, we set a circular buffer with a loose radius of 20 m. In this article, the streets with lights on only one side and those with lights on both sides are, respectively, termed as single light streets [see Fig. 5(a)] and double light streets [see Fig. 5(b)].

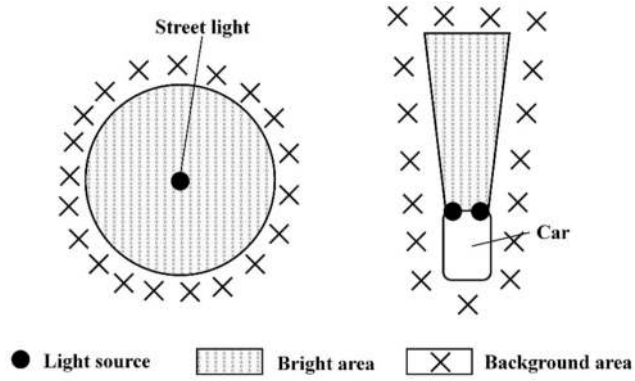

Fig. 6. Difference between street light and vehicle light.

For an area illuminated by only one street light, a pixel closer to the street light exhibits a higher brightness value. In addition, the pixel in the center of the street light may exhibit the maximum JL1-3B grayscale brightness, which implies that the pixels with local maximum value can be used to locate a street light. However, within the road area, there exist two light sources (street light and vehicle light). To enhance the accuracy of street light extraction, the vehicle light must be eliminated.

Because the vehicle light is directed in one direction, in contrast to street light, which is directed in all directions (see Fig. 6), the street light always could lit much larger area than the vehicle light. Thus, to avoid removing street light by mistake, the radius of sliding window of removing vehicle light must be smaller than that of extracting street light. The circular window with a radius of 5 m was considered as sliding for each pixel along with the street direction. The pixels with the lowest radiance values (89 nanowatts/cm^2/sr) were regarded as background pixels [29]. This threshold value was calculated from the minimum DN values (DN $=$ 1) of the three bands. If at least one background pixel existed in the sliding window, the entire window was regarded as a mask and eliminated for further extraction.

Because a street light could be located near the shared edge point of the adjacent JL1-3B pixels, the adjacent pixels could all have the highest nighttime light intensity as well as grayscale brightness. This situation could make the extraction result of the street light indicate more than one positions. Therefore, a mean filter was applied to smooth the JL1-3B grayscale brightness. Determining the scale of the mean filter and subsequent algorithms is a key issue, and it could affect the accuracy of the extraction results. Considering the distance between two street lights and street light radius, we set the value of this key parameter as 10 m (Section V-B discusses the sensitivity of this parameter). In the process of mean filtering, the value of the padding pixels was set as 0, which could avoid the light sources

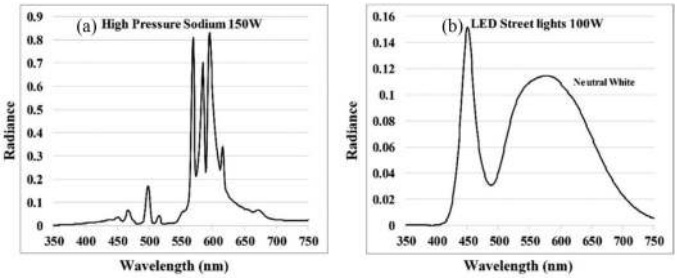

Fig. 7. Spectra of (a) HPS and (b) LED lamp.

at the edge of the study area being detected as street lights. Finally, a circular window with a radius of 10 m was used to determine all the local maximum grayscale brightness pixels, which were indicated as street lights.

HPS lamps and LED lamps are the main sources of road lighting within the study area. With reference to a previous study [34], the relationship between the radiance and wavelength of each type of lamp (see Fig. 7) was analyzed for the classification of the street light types. For instance, an HPS lamp has a dense cluster of strong emission from 569 to 616 nm, and the radiance is more than 0.6 at 569, 594, and 598 nm. At 500 nm, the spectra of the HPS lamp have a local peak and its radiance is close to 0.2. For an LED lamp, the highest radiance is at 450–460 nm with a local peak in the red band.

A pixel may contain more than one light source. To eliminate the influence from overlapped footprints, the training samples for street light classification must thus be free of any stray light. In this article, the samples of HPS and LED lamps were selected based on the field survey and their locations were recorded. According to the information of the three bands of JL1-3B, we used supervised classification to classify the types of street lights in the study area by using the maximum likelihood method because the maximum likelihood method has low computation cost and less time consuming. Half of the samples were used for the training classification model and the remaining samples were used to validate the model.

B. Assessment of Solar Street Light Utilization Potential

Because the solar street lights, which have a lower energy cost compared with that of traditional HPS street lights, have been increasingly focused on, we set up a scenario in which all the HPS street lights were replaced by solar street lights with LED lamps. The SHORTWAVE-C model was designed to estimate the direct, diffused, and reflected solar radiation, and the solar illumination duration was determined by using the DSM data and hourly cloud cover data considering the weather conditions [32], [35]. In this article, for each extracted street light position, the annual total solar radiation was accumulated from each 10-min interval of every single day in 2016. For more details of the SHORTWAVE-C model, please refer to [32].

To maximize the utilization efficiency of the solar street lights, the solar panels must be south facing and have the optimum title of 28° according to the latitude information of the study area (see Fig. 8) [36]. We calculated the total radiation received by

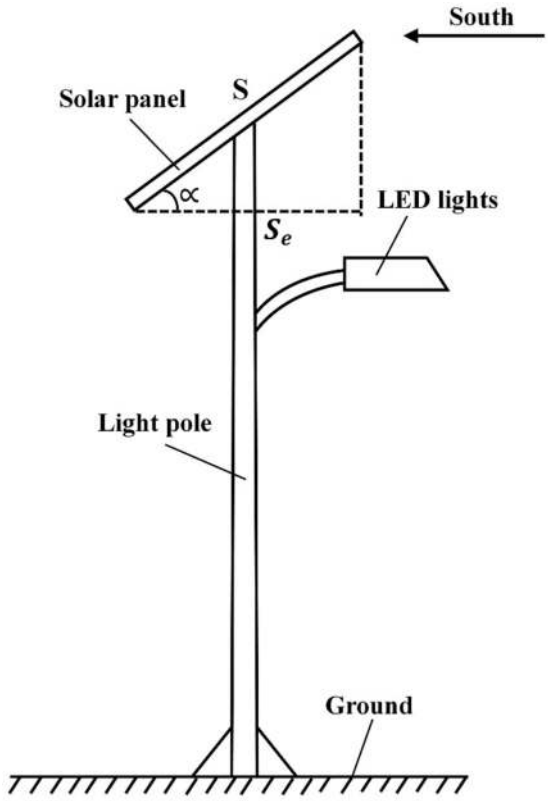

Fig. 8. Solar street light and solar panel installation.

each solar street light as

$$S_e = S \times \cos \propto \tag{2}$$

$$R = S_e \times R_s \tag{3}$$

where *S* represents the area of the solar panel; $\propto$ is the inclined angle for the solar panel; S_e is the effective area of one solar panel; R_s is the radiation per unit area received at the location of the street light, which can be calculated from SHORTWAVE-C model; and *R* is the total radiation received by one solar panel.

As it is difficult to correctly forecast the weather for the next 20 years, we have to assume that the weather condition during the life time of the solar street light (20 y) is the same as that in 2016 and regarded the estimated solar radiation of 2016 as the annual solar radiation for the next 20 y. The electricity generation in the *i*th year can be calculated using (4), and the total electricity generation for 20 years can be determined using (5)

$$E_i = \frac{R_i \times \eta_p \times \eta_s \times (1-\gamma)^{i-1}}{3.6} \tag{4}$$

$$E = \sum_{i=1}^{20} E_i \tag{5}$$

where R_i is the solar energy received by the solar panels in the *i*th year; γ is the attenuation coefficient of the solar street light system, assuming that the system efficiency is an equal series which drops by 17% per year, according to our market research [37]; η_p is the photoelectric conversion efficiency of the solar panels; η_s is the system efficiency, which is divided by 3.6 to

TABLE II
POWERS OF HPS AND LED LAMPS (UNIT: W)

Type	HPS (<8 m)	LED (<8 m)	HPS (>8 m)	LED (>8 m)
Power	250	60	400	90

TABLE III
EMISSION FACTOR PER KWH ELECTRICITY (UNIT: KG/KWH)

Standard coal	C emission	CO_2 emission	SO_2 emission	NO_X emission
0.4	0.272	0.997	0.03	0.015

convert the unit MJ to kWh; and E_i is the electricity generated by each solar street light. The photoelectric conversion efficiency of the solar panels is only 12% to 20% [38]–[40], and we set η_p as 15% in this article. At the same time, to account for the electrical energy loss during transmission, it is considered that approximately 85% (η_s) of the generated electrical energy can be used for lighting [41].

To accurately evaluate the solar street light utilization potential, it is important to determine the size of the solar panels. To fully exploit the energy, the size of the solar panels should be determined according to the energy consumed by the solar street lights. According to the Urban Road Lighting Design Standard in China, in most cases, the relationship between the powers of the HPS and LED lamps and height of the street light can be defined as listed in Table II. Because the study area is located in an urban area of Shanghai, the height of the street lamp is relatively low; we assumed that the height of the street lights is less than 8 m in the study area.

According to the annual average nighttime, a night in Shanghai lasts 11 h and 52 min. We used this duration as the daily average lighting time of the street light. From the aforementioned data, we can conclude that the daily energy requirement of one HPS lamp (E_h) is 10.68 MJ. Because solar street lights mainly use LED lamps, the daily energy requirement of one solar street light (E_s) is 2.56 MJ. For a solar street light, the optimum area of the solar panel (S) can be calculated as

$$S = \frac{E_s}{E_p} \tag{6}$$

where E_p is the daily electricity generation of per unit area of the solar panel.

In summary, we evaluated the environmental benefits based on the energy saved by solar street lights. The National Bureau of Statistics, in the context of the calculation of the standard coal coefficient states that 0.4-kg standard coal is required to produce 1 kWh electricity. Using the standard coal emission factor recommended by the Energy Research Institute of the National Development and Reform Commission, the carbon emission, CO_2 emission, SO_2 emission, and NO_X emission per kWh electricity can be obtained by using conversion rates specified in Table III. Subsequently, the quality of the ith emission factor reduction (Q_i) using solar lights can be calculated as

$$Q_i = \varnothing_i \times E \tag{7}$$

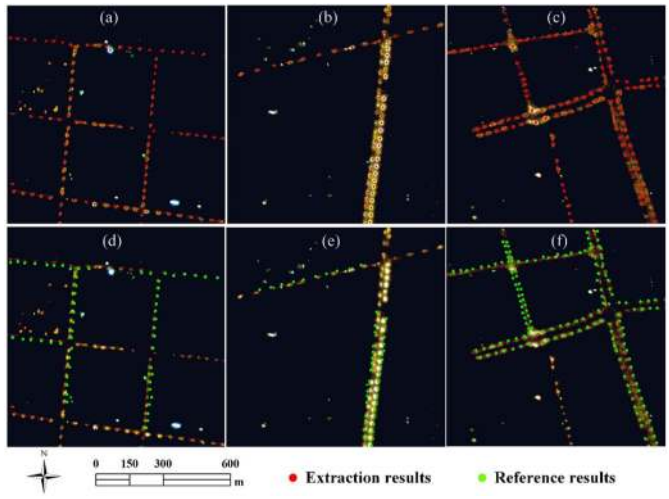

Fig. 9. Extraction and reference results of street lights from the three sample areas. (a) and (d) Area A. (b) and (e) Area B. (c) and (f) Area C.

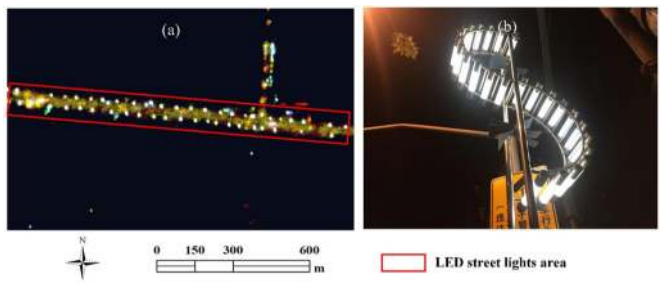

Fig. 10. (a) LED street lights on Gulang Road from JL1-3B nighttime light data and (b) the LED street light scene.

where $\varnothing_i$ represents the quality of the ith emission factor per kWh and E is the electrical energy generated by the solar street lights.

IV. RESULTS

A. Position and Types of Street Lights

In this article, we used the Python language to extract 4119 street lights, of which 111, 61, and 126 street lights were, respectively, located in areas A–C [red dots in Fig. 9(a)–(c)]. To assess the accuracy of the extraction results, we pinpointed a certain proportion of the street lights within the three sample areas in the field as the reference data. However, owing to road closure caused by infrastructure construction, only the accessible street light samples were retained, as shown in Fig. 9(d)–(f).

The HPS lamps dominated the study area and approximately 4045 HPS street lights were identified. Meanwhile, 74 LED lamps were detected on Gulang Road [see Fig. 10(a)]; the LED street light scene is shown in Fig. 10(b).

B. Utilization Potential of Solar Street Lights

Fig. 11(a)–(c) shows the annual average distribution of the total solar radiation in three sample areas. In the study area, the minimum and maximum solar radiation values are 1.97 and

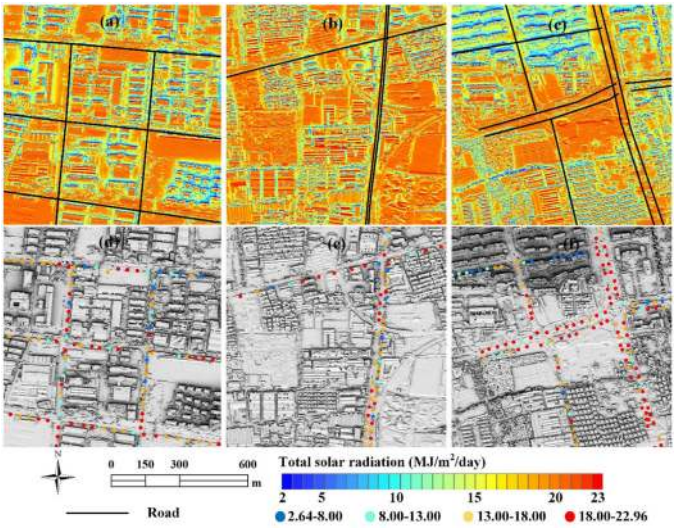

Fig. 11. Annual average total solar radiation of the entire area and the street lights in the three sample areas. (a) and (d) Area A. (b) and (e) Area B. (c) and (f) Area C.

TABLE IV
SOLAR POTENTIAL ASSESSMENT FOR ONE SOLAR STREET LIGHT

	Type I	Type II	Type III	Type IV
Annual average radiation (MJ/m2/day)	2.64-8.00	8.00-13.00	13.00-18.00	18.00-22.96
Electricity (kWh/m^2/day)	0.08-0.24	0.24-0.39	0.39-0.55	0.55-0.69
Area of solar panels Required (m2)	9.25-2.97	2.97-1.82	1.82-1.30	1.30-1.03

23.04 MJ/m^2/day, respectively. According to the DSM data, we found that buildings could easily block the road area receiving the solar radiance. For street lights [see Fig. 11(d) and (e)], the minimum and maximum values of the annual average radiation are 2.64 and 22.96 MJ/m^2/day, respectively. In area A, the annual average total solar radiation of the street lights is evenly distributed in four ranges. Street lights away from the buildings have a higher solar radiation, whereas those close to the buildings have a lower solar radiation. In area B, more than 13 MJ/m^2/day of annual average total solar radiation is received by most of the street lights because of the sparse building density. In area C, the street lights located in the northwest region receive low solar radiation (less than 8 MJ/m^2/day) because these street lights are located near a high-rise residential area. Furthermore, most of the remaining street lights receive more than 18 MJ/m^2/day of annual average total solar radiation.

The solar street lights are divided into four categories (types I–IV) based on the annual average total solar radiation received during the entire life time of the lamps (20 y). The daily electrical energy generated by the solar panels per unit area and the optimum area of the solar panel (S) for each type of solar street lamp can be calculated using (3)–(5) (see Table IV).

By replacing the HPS lamp, each solar street light can save 1.85×10^4 kWh of electrical energy, 7.41 t of standard coal, 5.03 t of C emissions, 18.47 t of CO_2 emissions, 0.55 t of SO_2 emissions, and 0.28 t of NO_X emissions for 20 y.

TABLE V
SOLAR POTENTIAL ASSESSMENT FOR SOLAR STREET LIGHTS IN TOTAL STUDY AREA (EXCLUDING LED STREET LIGHTS) AND AREAS A–C

	Study area	Area A	Area B	Area C
Electricity (10^6· kWH)	74.95	2.06	1.13	2.33
Standard coal (10^3·t)	29.98	0.82	0.45	0.93
C emission (10^3·t)	20.38	0.56	0.31	0.63
CO_2 emission (10^3·t)	74.70	2.05	1.13	2.32
SO_2 emission (t)	2244.85	61.73	33.81	69.93
NO_X emission (t)	1139.69	30.86	16.91	34.96

TABLE VI
RATE OF CORRECT IDENTIFICATION OF STREET LIGHTS

	Area A	Area B	Area C
Number of samples	67	47	121
Correctly identified samples	64	42	112
Accuracy	95.5%	89.4%	92.6%
Average error (m)	6.43	8.27	5.31

Table V presents the total amount of generated electricity and the total environmental benefits during the entire life time of the lamps (20 y). Excluding the existing LED street lights, all the solar street lights can save up to 7.50×10^7 kWh of electrical energy, 3.00×10^4 t of standard coal, 2.04×10^4 t of C emissions, 7.47×10^4 t of CO_2 emissions, 2.24×10^3 t of SO_2 emissions, and 1.14×10^3 t of NO_X emission in the entire study area for 20 y.

V. DISCUSSION

A. Accuracy Assessment

The reference street light data from field survey in the three sample areas were applied to evaluate the extraction results. If the distance between an extraction result and the corresponding reference street lamp position was within 10 m (location error), we believed that this extraction result was correct and acceptable. The accuracy of the extracted street light position in each sample area was approximately 90%, as presented in Table VI. The average error indicates the average distance between the extracted and reference street lights within a sample area.

The results in Fig. 9 and Table VI indicate that the street light extraction on a single light street demonstrates better accuracy. For example, the overall accuracy of area A is 95.5% with a low average error of 6.43 m. Area B includes both single light streets and double light streets. The street lights on single light streets were extracted well, whereas the street lights on the double light streets corresponded to a lower extraction accuracy. Owing to this complex street light pattern, the accuracy of area B was the worst among the three sample areas, even though its value was almost 90%. Area C contains many complex roads and several junctions. In the single light street, the proposed method exhibits a satisfactory accuracy, whereas in the case of the double light street, street lights on only one side were found because the street lights are too close to each other [see Fig. 9(c) and (f)]. This finding indicates that the proposed method exhibits

TABLE VII
RATE OF CORRECT DISCRIMINATION OF STREET LIGHT TYPES

	Omission error	Commission error
HPS	0.05%	0.32%
LED	15.29%	2.70%

TABLE VIII
SENSITIVITY ANALYSIS OF EXTRACTION RESULTS

Threshold	Area A	Area B	Area C
8 m	94.0%	89.4%	89.3%
9 m	97.0%	89.4%	90.9%
10 m	95.5%	89.4%	92.6%
11 m	94.0%	85.1%	92.6%
12 m	92.5%	80.9%	91.7%

different accuracies in single and double light streets. Overall, the approach is suitable for complex road networks.

It is worth noting that some street lights in our study area were ignored owing to the coverage of the trees. However, the purpose of this study was to evaluate the potential of the solar street lights. The street lights covered by trees likely receive a low amount of solar radiance and are not necessary to be replaced as solar street lights. Therefore, these street lights were not considered for further analysis.

Table VII presents the accuracy of the street light type discrimination in the study area. The total corresponding accuracy was 99.64%. Compared with HPS lamps, the fewer numbers of LED lamps led to high omission and commission errors.

B. Sensitivity Analysis of Extraction Results

In Section III-A, we extracted the position of the street lights in our study area by using the local maximum method. In this process, we chose a circle with a radius of 10 m as the sliding window. As an important threshold parameter, we must understand how this parameter impacts the accuracy of street light extraction. A sensitivity analysis of this parameter was thus conducted, as summarized in Table VIII. The parameter increased from 8 to 12 m with a step of 1 m, which corresponded to almost the same extraction results in areas A–C. With a low threshold value, there may be two extraction results in one street lighting range. With a high threshold value, it is likely that only half the street lights on a double light street may be extracted. This sensitivity analysis indicates that the change in the threshold value could influence the extraction results to only a small degree. This also means that the window size is a key parameter for this article, but using 10 m as the radius is suitable for most areas. Irrespective, an appropriate threshold value is still essential when using the proposed method for the extraction of street lights.

C. Suggestions Regarding Solar Street Lights

According to Section IV-B, a solar street light in an appropriate position can generate a considerable amount of electrical energy and garner several environmental benefits during its service life. Using the JL1-3B nighttime light data, DSM data and hourly cloud cover data, we can accurately calculate the electrical energy and environmental benefits generated by solar street lights at each location for 20 y. At the same time, the optimum area of the solar panels can be calculated for each solar street, which can guide the suitable installation of solar street lights.

According to the four types of solar street lights mentioned in Section IV-B, the government can customize four sizes of solar panels. To ensure the power supply of solar street lights, the maximum area of the corresponding type should be selected. Because the area of type I (9.25–2.97 m^2) exceeds the reasonable range, and it is likely that the street light is blown down by strong wind, we do not recommend the installation of type I solar street lights. At the locations of types II-IV solar street lights, the area of the solar panels can be customized to 2.97, 1.82, and 1.30 m^2, respectively. In the case of area C for example, we can abandon the type I street lights in the northwest region that receives less solar radiation, and use compatible solar street lights in the regions that receive a high solar radiation. Compared with a wide range of indiscriminate installations, the optimal installation of solar street lights can reduce costs and maximize the potential of solar energy.

In practical applications, the solar panels can be designed to adjust the inclined angle and direction according to the incident direction of the sunlight. Meanwhile, the size of the solar panels can also be adjusted considering the actual power consumption of the street lights. By combining the abovementioned aspects, solar street lights can provide greater benefits in urban energy conservation.

D. Limitations

In this article, the considered DSM data and hourly cloud cover data corresponded to 2016, whereas the JL1-3B nighttime light data corresponded to 2017. If new constructions are established between 2016 and 2017, the DSM data will be changed. But this change could only influence the solar radiance assessment and could not affect the accuracy of street light extraction and classification. To obtain a precise assessment of the potentials of solar street lights, an up-to-date DSM data are required.

Furthermore, owing to the inclination of JL1-3B, high-rise buildings, trees, and large billboards would disrupt the recording of the nearby street lighting, which is a difficult problem to be addressed. Therefore, considerable work is still required to develop a more accurate approach for the assessment of solar street light potential.

The potential of solar street lights was assessed without considering the occurrence of extreme weather, even though the weather condition can influence the utilization of the solar street lights. To make the street light safer and more sustainable, we think an emergency power supply is required for the solar street lights.

VI. CONCLUSIONS

In this article, we introduced an approach to extract street lights and assess their solar energy potential by using the JL1-3B nighttime light data. First, we determined the position of the

street lights by using the local maximum method from the OSM data and JL1-3B nighttime light data. The accuracy of the extraction results in the three sample areas was approximately 90%. Using the multispectral characteristics of the JL1-3B nighttime light data, we determined the difference between the HPS lamps and LED lamps and extracted the LED street lights in the considered study area. By performing field visits, we confirmed the correctness of the LED street lights extracted using the JL1-3B nighttime light data. Then, we used the DSM data and hourly cloud cover data to build a SHORTWAVE-C model and obtained the annual average total solar radiation distribution in the study area. Next, we obtained the annual average total solar radiation of all the street lights (except LED street lights) in the study area and simulated their replacement with solar street lights. After certain modifications (for example, in terms of unit conversions), we proposed a refined installation scheme for each type of solar street lights. Furthermore, we highlighted the electrical energy generation and environmental benefits pertaining to the use of solar street lights in our study area. Combining the results of the three sample areas, we provided suggestions for the optimal installation of solar street lights and believe that this article can provide scientific guidance for the popularization of solar street lights.

In summary, our method has three advantages, namely the precise and efficient extraction of the street light usage data, the individual assessment of solar street light potentials, and the applicability to other regions.

REFERENCES

[1] N. Zhou, D. Fridley, N. Z. Khanna, J. Ke, M. Mcneil, and M. Levine, "China's energy and emissions outlook to 2050: Perspectives from bottom-up energy end-use model," *Energy Policy*, vol. 53, no. 53, pp. 51–62, 2013.

[2] T. V. Ramachandra and B. V. Shruthi, "Spatial mapping of renewable energy potential," *Renew. Sustain. Energy Rev.*, vol. 11, no. 7, pp. 1460–1480, 2007.

[3] S. R. Bull, "Renewable energy today and tomorrow," (in English), *Proc. IEEE*, vol. 89, no. 8, pp. 1216–1226, Aug. 2001.

[4] Y. Yang, "Energy saving and consumption reduction—A new perspective of urban lighting master plan: The practice and research on Hang Zhou urban green lighting master plan during the period of the 11th-five-year Plan," *China Illum. Eng. J.*, vol. 19, no. 3, pp. 12–17, 2008.

[5] G. Newman *et al.*, "Smarter shrinkage: A neighborhood-scaled rightsizing strategy based on land use dynamics," *J. Geovisualiz. Spatial Anal.*, vol. 2, no. 2, 2018, Art. no. 11.

[6] Y. Liu, L. Liu, and J. Tang, "Analyzing the application mode of solar lights in urban lighting system," *China Illum. Eng. J.*, vol. 25, no. 5, pp. 65–67, 2014.

[7] Y. Weng, "Application analysis and prospects of the high pressure sodium lamp and LED in the urban road lighting," *China Light Lighting*, no. 4, pp. 17–21, 2012.

[8] M. Ali, M. Orabi, E. Abdelkarim, J. A. A. Qahouq, and A. E. Aroudi, "Design and development of energy-free solar street LED light system," in *Proc. Innov. Smart Grid Technol.- Middle East*, 2012, pp. 1–7.

[9] W. X. Zeng, M. Jie, and Z. Ying, "Rapid charge system for lead-acid battery of solar energy street light based on single-chip microcomputer," in *Proc. Int. Conf. Comput. Sci. Inf. Technol.*, 2008, pp. 337–341.

[10] A. Kama, M. Diallo, M. S. Drame, M. L. Ndiaye, A. Ndiaye, and P. A. Ndiaye, "Monitoring the performance of solar street lights in Sahelian environment: Case study of Senegal," in *Proc. 10th Int. Conf. Develop. eSyst. Eng.*, Paris, France, 2017, pp. 56–61.

[11] F. J. Nogueira, L. A. Vitoi, L. H. Gouveia, and C. G. Casagrande, "Street lighting LED luminaires replacing high pressure sodium lamps: Study of case," in *Proc. IEEE/IAS Int. Conf. Ind. Appl.*, 2014, pp. 1–8.

[12] Y. Yu, J. Li, H. Guan, C. Wang, and J. Yu, "Semiautomated extraction of street light poles from mobile LiDAR point-clouds," *IEEE Trans. Geosci. Remote Sens.*, vol. 53, no. 3, pp. 1374–1386, Mar. 2015.

[13] W. Zhen *et al.*, "A multiscale and hierarchical feature extraction method for terrestrial laser scanning point cloud classification," *IEEE Trans. Geosci. Remote Sens.*, vol. 53, no. 5, pp. 2409–2425, May 2015.

[14] B. Rodríguez-Cuenca, S. García-Cortés, C. Ordóñez, and M. C. Alonso, "Automatic detection and classification of pole-like objects in urban point cloud data using an anomaly detection algorithm," *Remote Sens.*, vol. 7, no. 10, pp. 12680–12703, 2015.

[15] D. Zai, Y. Chen, J. Li, Y. Yu, W. Cheng, and H. Nie, "Inventory of 3D street lighting poles using mobile laser scanning point clouds," in *Proc. Geosci. Remote Sens. Symp.*, 2015, pp. 573–576.

[16] B. Yang and D. Zhen, "A shape-based segmentation method for mobile laser scanning point clouds," *ISPRS J. Photogram. Remote Sens.*, vol. 81, no. 7, pp. 19–30, 2013.

[17] B. Yang, D. Zhen, Z. Gang, and W. Dai, "Hierarchical extraction of urban objects from mobile laser scanning data," *ISPRS J. Photogram. Remote Sens.*, vol. 99, pp. 45–57, 2015.

[18] W. Fan *et al.*, "Rapid localization and extraction of street light poles in mobile LiDAR point clouds: A supervoxel-based approach," *IEEE Trans. Intell. Transp. Syst.*, vol. 18, no. 2, pp. 292–305, Feb. 2017.

[19] Y. Yu, J. Li, H. Guan, W. Cheng, and J. Yu, "Semiautomated extraction of street light poles from mobile LiDAR point-clouds," *IEEE Trans. Geosci. Remote Sens.*, vol. 53, no. 3, pp. 1374–1386, Mar. 2015.

[20] Y. Yu, J. Li, H. Guan, F. Jia, and C. Wang, "Three-dimensional object matching in mobile laser scanning point clouds," *IEEE Geosci. Remote Sens. Lett.*, vol. 12, no. 3, pp. 492–496, Mar. 2015.

[21] K. Shi, C. Huang, B. Yu, B. Yin, Y. Huang, and J. Wu, "Evaluation of NPP-VIIRS night-time light composite data for extracting built-up urban areas," *Remote Sens. Lett.*, vol. 5, no. 4, pp. 358–366, 2014.

[22] C. Li, G. Chen, J. Luo, S. Li, and J. Ye, "Port economics comprehensive scores for major cities in the Yangtze Valley, China using the DMSP-OLS night-time light imagery," *Int. J. Remote Sens.*, vol. 38, no. 21, pp. 6007–6029, 2017.

[23] C. Li, G. Li, Y. Zhu, Y. Ge, H.-T. Kung, and Y. Wu, "A likelihood-based spatial statistical transformation model (LBSSTM) of regional economic development using DMSP/OLS time-series nighttime light imagery," *Spatial Statist.*, vol. 21, pp. 421–439, 2017.

[24] C. Wang *et al.*, "Analyzing parcel-level relationships between Luojia 1-01 nighttime light intensity and artificial surface features across Shanghai, China: A comparison with NPP-VIIRS data," *Int. J. Appl. Earth Observ. Geoinf.*, vol. 85, 2020, Art. no. 101989.

[25] Y. Wei, H. Liu, W. Song, B. Yu, and C. Xiu, "Normalization of time series DMSP-OLS nighttime light images for urban growth analysis with pseudo invariant features," *Landscape Urban Planning*, vol. 128, no. 128, pp. 1–13, 2014.

[26] Z. Chen *et al.*, "A new approach for detecting urban centers and their spatial structure with nighttime light remote sensing," *IEEE Trans. Geosci. Remote Sens.*, vol. 55, no. 11, pp. 6305–6319, Nov. 2017.

[27] C. Li, L. Zou, Y. Wu, and H. Xu, "Potentiality of using Luojia1-01 night-time light imagery to estimate urban community housing price—A case study in Wuhan, China," *Sensors (Basel)*, vol. 19, no. 14, Jul. 2019, Art. no. 3167.

[28] G. Zhang, L. Li, Y. Jiang, X. Shen, and D. Li, "On-orbit relative radiometric calibration of the night-time sensor of the Luojia1-01 satellite," *Sensors (Basel)*, vol. 18, no. 12, Dec. 2018, Art. no. E4225.

[29] Q. Zheng *et al.*, "A new source of multi-spectral high spatial resolution night-time light imagery—JL1-3B," *Remote Sens. Environ.*, vol. 215, pp. 300–312, 2018.

[30] Y. Katz and N. Levin, "Quantifying urban light pollution—A comparison between field measurements and EROS-B imagery," *Remote Sens. Environ.*, vol. 177, pp. 65–77, 2016.

[31] M. Wang, Q. Li, Q. Hu, and M. Zhou, "Quality analysis of open street map data," in *Proc. Int. Arch. Photogram., Remote Sens. Spatial Inf. Sci.*, 2013, vol. XL-2/W1, pp. 155–158.

[32] Y. Huang *et al.*, "Estimating roof solar energy potential in the downtown area using a GPU-accelerated solar radiation model and airborne lidar data," *Remote Sens.*, vol. 7, no. 12, pp. 17212–17233, 2015.

[33] M. Grundland and N. A. Dodgson, "Decolorize: Fast, contrast enhancing, color to grayscale conversion," *Pattern Recognit.*, vol. 40, no. 11, pp. 2891–2896, 2007.

[34] C. D. Elvidge, D. M. Keith, B. T. Tuttle, and K. E. Baugh, "Spectral identification of lighting type and character," *Sensors*, vol. 10, no. 4, pp. 3961–3988, 2010.

[35] J. Zhang, Q. Zhou, X. Shen, and Y. Li, "Cloud detection in high-resolution remote sensing images using multi-features of ground objects," *J. Geovisualiz. Spatial Anal.*, vol. 3, no. 2, p. 14, 2019.
[36] D. Zhu and D. Yan, "Calculation of solar radiation and generated energy on inclined plane and optimal inclined angle," *Build. Sci*, vol. 28, pp. 277–280, 2012.
[37] Y. Li, "Assessment of solar energy utilization potential on building roof top: a case study of downtown Shanghai," Master's thesis, East China Normal Univ., Shanghai, China, 2019.
[38] L. Wiginton, H. T. Nguyen, and J. M. Pearce, "Quantifying rooftop solar photovoltaic potential for regional renewable energy policy," *Comput. Environ. Urban Syst.*, vol. 34, no. 4, pp. 345–357, 2010.
[39] M. A. Green, K. Emery, Y. Hishikawa, and W. Warta, "Solar cell efficiency tables (version 37)," *Progr. Photovolt., Res. Appl.*, vol. 19, no. 1, pp. 84–92, 2011.
[40] A. Nicholls, R. Sharma, and T. Saha, "Financial and environmental analysis of rooftop photovoltaic installations with battery storage in Australia," *Appl. Energy*, vol. 159, pp. 252–264, 2015.
[41] S. Choice, Optimizing Solar Panel System Efficiency Through Inverter Sizing, 2011. Available at: http://www.solarchoice.net.au/blog/optimizing-solar-panel-system-efficiency-through-inverter-sizing/l

Bin Cheng received the B.S. degree in remote sensing science and technology from the Nanjing University of Information Science and Technology, Nanjing, China, in 2017. He is currently working toward the M.S. degree in cartography and geographic information system with East China Normal University, Shanghai.

His research interests include the nighttime light remote sensing and its application in urban research.

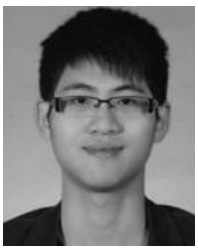

Zuoqi Chen (Member, IEEE) received the B.S. degree in geographic information system from Fujian Normal University, Fuzhou, China, in 2011, and the Ph.D. degree in cartography and geographic information system from East China Normal University, Shanghai, China, in 2017.

He is currently an Assistant Research Fellow with the Key Laboratory of Spatial Data Mining and Information Sharing of Ministry of Education, and the Academy of Digital China, Fuzhou University, Fuzhou. His research interests include urban remote sensing, nighttime light remote sensing, and development of geographic information system.

Bailang Yu (Senior Member, IEEE) received the B.S. and Ph.D. degrees in cartography and geographic information systems from East China Normal University, Shanghai, China, in 2002 and 2009, respectively.

He is currently a Professor with the Key Laboratories of Geographic Information Science, Ministry of Education, and the School of Geographic Sciences, East China Normal University. His research interests include urban remote sensing, nighttime light remote sensing, LiDAR, and object-based methods.

Qiaoxuan Li received the B.S. and M.S. degrees in cartography and geographic information system from Fujian Normal University, Fuzhou, China, in 2015 and 2018, respectively. He is currently working toward the Ph.D. degree in cartography and geographic information system with East China Normal University, Shanghai, China.

His research interests include nighttime light remote sensing and its application in urban research.

Congxiao Wang received the B.S. and M.S. degrees in cartography and geographic information system from Shanghai Normal University, Shanghai, China, in 2014 and 2017, respectively. She is currently working toward the Ph.D. degree in cartography and geographic information system with East China Normal University, Shanghai.

Her research interests include nighttime light remote sensing and its application in urban research.

Beibei Li received the B.S. degree in satellite photography from Wuhan University, Wuhan, China, in 2015.

He is currently an Assistant Research Fellow with the Changchun Institute of Optics, Fine Mechanics and Physics, Chinese Academy of Sciences, Changchun, China, and Chang Guang Satellite, Changchun. His research interests include industrialization of remote sensing application and satellite data processing.

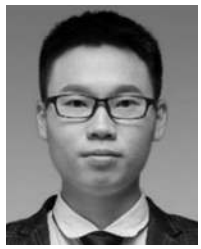

Bin Wu received the Ph.D. degree in cartography and geographic information systems from East China Normal University, Shanghai, China, in 2018.

He is currently a Postdoctoral Researcher with the East China Normal University. His fields of interests are urban remote sensing, LiDAR, and spatiotemporal analysis.

Yong Li received the B.S. degree in science of geography from Huazhong Agricultural University, Wuhan, China, in 2016, and the M.S. degree in cartography and geographic information system from East China Normal University, Shanghai, China, in 2019.

His research interests include the nighttime light remote sensing and its application in urban research.

Jianping Wu received the M.S. degree in cartography and remote sensing from Peking University, Beijing, China, in 1986, and the Ph.D. degree in regional geography from East China Normal University, Shanghai, China, in 1996.

He is currently a Professor with East China Normal University. His research interests include remote sensing and geographic information system.